Ann. Geophys., 31, 473–487, 2013
www.ann-geophys.net/31/473/2013/
doi:10.5194/angeo-31-473-2013

Annales Geophysicae
Open Access

The Geminid meteor shower during the ECOMA sounding rocket campaign: specular and head echo radar observations

G. Stober[1], **C. Schult**[1], **C. Baumann**[1,*], **R. Latteck**[1], **and M. Rapp**[1,*]

[1]Leibniz-Institute of Atmospheric Physics at the Rostock University, Schlossstr. 6, 18225 Kühlungsborn, Germany
[*]now at: German Aerospace Center (DLR), Institute of Atmospheric Physics, Münchner Straße 20, 82234 Oberpfaffenhofen-Wessling, Germany

Correspondence to: G. Stober (stober@iap-kborn.de)

Received: 28 July 2012 – Revised: 19 February 2013 – Accepted: 25 February 2013 – Published: 12 March 2013

Abstract. The ECOMA (Existence of Charge state Of meteoric smoke particles in the Middle Atmosphere) sounding rocket campaign was conducted during the Geminid meteor shower in December 2010 in order to explore whether there is a change of the properties of meteoric smoke particles due to the stream. In parallel to the rocket flights, three radars monitored the Geminid activity located at the launch site in Northern Norway and in Northern Germany to gain information about the meteor flux into the atmosphere. The results presented here are based on specular meteor radar observations measuring the radiant position, the velocity and the meteor flux into the atmosphere during the Geminids. Further, the MAARSY (Middle Atmosphere Alomar Radar System) radar was operated to conduct meteor head echo experiments. The interferometric capabilities of MAARSY permit measuring the meteor trajectories within the radar beam and to determine the source radiant and geocentric meteor velocity, as well as to compute the meteor orbit.

Keywords. Atmospheric composition and structure (Middle atmosphere – composition and chemistry) – Interplanetary physics (Interplanetary dust) – Ionosphere (Ion chemistry and composition)

1 Introduction

The ECOMA sounding rocket campaign was conducted during December 2010. The major objective was to provide quantitative in situ measurements of meteoric smoke particles (MSP) before, during and after a major meteor shower and to relate changes in the chemical structure or number densities of the MSPs to the changed meteor mass input into earth's atmosphere.

Therefore, the meteor activity was monitored using standard specular meteor radars to determine the source radiant activity, the sporadic meteor background and to estimate the particle sizes/masses of the incoming meteoroids. The observations were conducted at two different latitudes to gain more general information about the Geminid meteor shower characteristics. Close to the launch site in Northern Norway (69.1° N, 16° E), the new High-Power Large-Aperture (HPLA) radar MAARSY (Middle Atmosphere Alomar Radar System) and a standard meteor radar were operated to observe the meteor flux in almost the same volume as probed by the rockets. The horizontal distance of the radar from the launch pad is approximately 1 km. The second station that was involved in the campaign of the Geminid meteor shower is at Juliusruh (54.6° N, 13.4° E), Germany, which is approximately 15° South of the latitude of the launch site.

The Geminid meteor shower is the most prominent meteor stream throughout the year for specular radar observations in the Northern Hemisphere and shows basically comparable characteristics with the sporadic meteor background concerning the altitude and velocity distribution. The shower has a geocentric velocity of 35 km s^{-1} (e.g. Dudnik et al., 1959; McKinley, 1961) and typical stream particles form a detectable meteor trail at an altitude range similar to most of the sporadics. Typical Geminids occur in the altitude range between 85–95 km (specular observation). Therefore, one would expect that this shower provides a significant source of meteoric raw material that can condense to nanometer sized particles at the altitude range where most of the MSPs exist (Megner et al., 2006, 2008). Specular radar observations

Table 1. Technical details of the used meteor radars. The abbreviation PRF stands for pulse repetition frequency.

Parameter	Andenes	Juliusruh
Location	69.1° N, 16° E	54.6° N, 13.4° E
Frequency	32.55 MHz	32.55 MHz
PRF	2094 Hz	2144 Hz
Coherent integrations	4	4
Peak power	30 kW	15 kW
Antenna	crossed dipole	crossed dipole
Pulse length	13 µs	13 µs
Range resolution	2 km	2 km

of the Geminids have shown over decades that the shower significantly exceeds the sporadic meteor flux and indicates only a weak inter-annual variability comparing previous and recent works on this meteor shower (e.g. Jones and Morton, 1982; Brown et al., 1998; Stober et al., 2011).

One aim of this study is to infer absolute meteor fluxes for the Geminids using specular radar observations to estimate the mass input in the mesosphere/lower thermosphere (MLT) for the observed particles sizes/masses. Therefore, the approach presented in Campbell-Brown and Jones (2006), which is based on Kaiser's theory (Kaiser, 1960) is used to estimate the effective radar collecting area. The meteor flux estimates are compared to the mass fluxes predicted by Ceplecha et al. (1998); Love and Brownlee (1993) and Rietmeijer (2000) for particles of the same size/mass interval.

While, it is not intended to derive an absolute mass input covering a huge particle size range from the specular radar data, the measurements are useful to reduce the large uncertainties of the meteoric mass flux into the atmosphere. The radar observations represent at least a lower boundary of the meteor mass input into the atmosphere for the detected particles sizes. Mathews et al. (2001) estimated the meteoric mass flux into the atmosphere from Arecibo radar observations (meteor head echo) to be of the order of $5\,\mathrm{t\,d^{-1}}$, which is significantly lower than the derived meteoric flux of $270\,\mathrm{t\,d^{-1}}$ from Zodiacal dust cloud measurements (Nesvorný et al., 2010).

This study is structured as follows. The second section described the radars that were used during the campaign and provides the information about the relevant experiment parameters. The third section focuses on specular radar data and the measurement of the radiant activity, meteor velocity and mass determination as applied in this study. The fourth section is attributed to the conducted MAARSY head echo observations, which includes the description of the interferometric capabilities of MAARSY and the characteristics of the Geminid meteor shower based on the two different radar methods concerning vector velocity, altitude and source radiant measurements. In Sect. 5 we present the main conclusions that we derived from these observations.

Table 2. MAARSY system parameters used for the meteor head experiment. The abbreviations PRF stands for pulse repetition frequency and IPP means inter- pulse period.

Parameter	Meteor experiment
PRF	700 Hz
Coherent integrations	1
Pulse length	48 µs
IPP	1.43 ms
Duty cycle	3.36 %
Sampling start range	72.9 km
Sampling end range	148.5 km
Sampling resolution	900 m
Sampling rate	6 µs
Range gates	85
Number of data points	8192
Time resolution dt	1.43 ms

2 Radars

The specular meteor radar (MR) observations were conducted using two all-sky SKiYMET radars (Hocking et al., 2001). One radar is situated close to the Andøya Rocket Range and the second one is a mid-latitude station at the Baltic sea coast in Northern Germany. Both radars use an identical software and crossed dipole antennas on transmission and reception. This ensures an almost symmetrical antenna pattern (Singer et al., 2004). A detailed list of the experimental parameters is given in Table 1.

In addition to these standard meteor experiments both radars were calibrated using the delay line method (Latteck et al., 2008). This permits to directly quantify the observed electron line densities in order to estimate the meteoroid size/mass assuming single body meteor ablation. This is of particular importance for the derived meteor fluxes.

The head echo observations were conducted with MAARSY. This radar operates at 53.5 MHz and is located approximately 1 km northeast of the rocket launch site at the Andøya Rocket Range. For the meteor head echo experiment analyzed in this study, we employed a vertical beam and transmitted pulses of 48 µs without applying pulse coding. On reception, 8 channels of the multi-channel recording system were used. One channel was reserved for the complete available array. The remaining 7 channels were connected to smaller sub-arrays, which each consisted of 49 antennas and are further called "anemones" within this paper. A summary of the experiment parameters is listed in Table 2.

The positions of all 7 sub-arrays are shown in Fig. 11. All antennas with the same color code ("anemone") are connected to the same receiver channel. Each "anemone" consists of 49 antennas. The xy position is defined by the center coordinates of each sub-array. All antenna cables are phase matched and agree within 1°. The grey rectangles at the perimeter of the system indicate the position of the

equipment buildings hosting the transceiver modules and the labels A–F stand for the MAARSY antenna sub-structures to ensure an equal length of all phase matched cables. The antenna groups of seven antennas that are not color coded were not in use during the campaign. MAARSY was operated using the second stage of expansion, which consisted of 343 TRx modules (Latteck et al., 2012a). Hence, the total peak power of the system was approximately 680 kW. This second stage of expansion lead to a beam width of 4.2°. Although there is a distance of 28 m between all sub-arrays, the ambiguity zones are still larger than the main beam width. These ambiguity zones (green) and the minimum in radiation pattern between the main beam and the first side lobe are shown in Fig. 12a). The red lines in this view graph represent minima in the radiation pattern and separate the main beam from the first side lobe, which is almost symmetric. More details about the head echo experiment are given in Sect. 4.

3 Specular radar observations

Specular meteor observation have been conducted for decades (e.g. Öpik, 1958; McKinley, 1961; Jones and Morton, 1982; Brown et al., 1998; Hocking et al., 2001; Campbell-Brown and Jones, 2006; Stober et al., 2011). Nowadays, specular meteor observations together with the recent generation of meteor radars are mainly designed to measure upper atmosphere winds and temperatures (e.g. Hocking et al., 2001; Singer et al., 2003, 2004). However, the potential of these meteor radars to investigate astrophysical meteor parameters has been also an important task since the beginning of the observations. These radars have proven to be a valuable tool to study meteor source radiants (e.g. Hocking et al., 2001; Campbell-Brown and Jones, 2006; Jones et al., 2005; Jones and Jones, 2006) and entry velocity and masses (e.g. Baggaley et al., 1994, 1997; Brown et al., 1998; Hocking, 2000; Baggaley, 2002; Stober et al., 2011).

3.1 The radiant activity

The radiant activity during the Geminid meteor shower was monitored by applying a single station radiant mapping method presented in Jones and Jones (2006). This technique basically utilizes the geometry of the specular meteor observation by computing the radial radar vector $\boldsymbol{R}$, which is defined as the vector from the radar towards the specular point of the meteor trail. The source radiant for this meteor trail must lie within a great circle (GC), which is defined by all vectors perpendicular to the radar vector $\boldsymbol{R}$.

Jones and Jones (2006) suggested to compute a weighted scalar product between a set of trial radiants with the radar vector for each meteor trail. The basic idea of this method is that for all trial vectors $\boldsymbol{T}$, which are close to this GC the weighted scalar product vanishes

$$0 \approx \int_{\mathrm{GC}} w(\boldsymbol{T} \cdot \boldsymbol{R}) d\phi \quad . \tag{1}$$

The trial radiant $\boldsymbol{T}$ can be any vector defined by the unit circle. Here we used a $2^\circ \times 2^\circ$ grid to compute the scalar product. The weighting function w is composed of one acceptance and two rejection bands in such a way that the integral over the complete hemisphere vanishes (Jones and Jones, 2006). The introduction of two rejections bands in the direct vicinity of acceptance band removes the diffuse halo, which is created by just having one acceptance band (e.g. using a "top-hat" function). The weighting function used in this work is a composite of three Gaussian functions with a standard deviation of $\sigma = 4^\circ$, which corresponds to a width of the acceptance band of 2°. In Fig. 1 a three-band-top-hat weighting function is compared to three-band Gaussian.

Applying such a three band function leads to two effects. Firstly, this weighting function suppresses all sources that are much larger than the used convolution width. The smaller the width of the acceptance band the stronger the filter effect of all diffuse meteor sources. Hence, such a small acceptance band is ideal to identify meteor streams. The more diffuse sporadic meteor sources are suppressed by the rejection bands. Secondly, the overall sum of the activity map remains zero, which means that there are areas on the celestial sphere with negative radiant activity. These negative values are considered as noise (Jones and Jones, 2006).

The radiant activity maps presented here are computed on the basis of a $2^\circ \times 2^\circ$ grid structure of trial radiants in celestial coordinates covering the complete hemisphere. However, to remove the GC ambiguity only meteor trial radiants above the horizon are accumulated into the radiant activity map. The shown radiant activity maps are computed using all available meteor detections at the appropriate day.

In Fig. 2 the radiant activity for all three ECOMA sounding rocket flights are shown. The color bar on the right side indicates an arbitrary intensity and does not allow estimating the absolute number of meteors, which originated from a certain source radiant. Further, these plots are created using the complete ensemble of meteors during 24 h of observation. Hence, the graphs shown in Fig. 2 represent average daily radiant activities.

The first rocket was launched on 4 December 2010. At this time the sporadic meteor background was still dominating the radiant activity map. However, it is already possible to see also some weak activity generated by the Geminids. The second flight was conducted on 13 December shortly before the Geminids reached their absolute peak activity. The radiant activity map for this flight is completely dominated by the Geminid meteor shower. The final ECOMA sounding rocket flight lifted off on 19 December. During this time the Geminid shower had already vanished. The remaining radiant activity is mainly generated by the sporadic background.

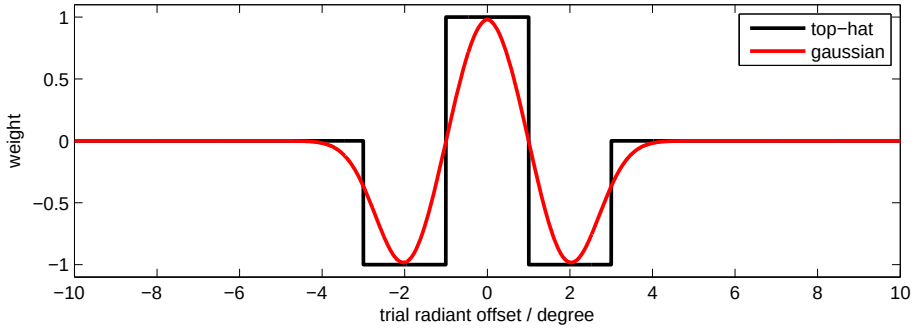

Fig. 1. Comparison of two three band radiant weighting functions.

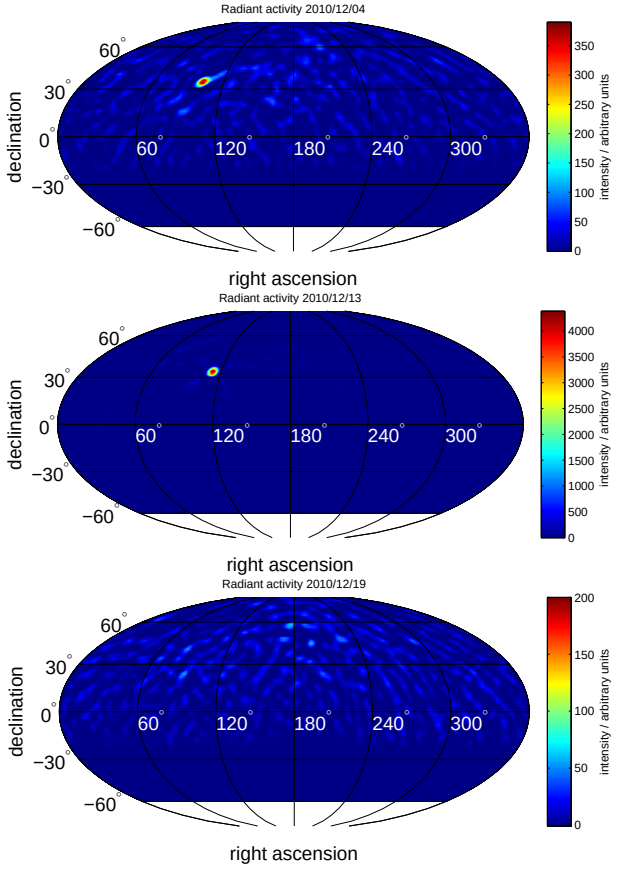

Fig. 2. Radiant activity maps during all three ECOMA sounding rocket flights measured with the Andenes meteor radar.

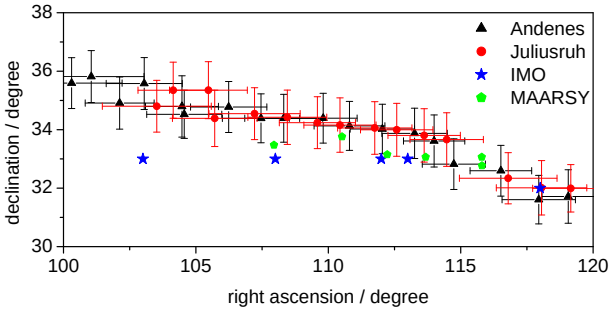

Fig. 3. Radiant position of the Geminid meteor shower for the Andenes and Juliusruh MR, IMO and MAARSY head echo observations.

The radiant activity maps were also analyzed to determine the radiant position and the apparent motion of the Geminid source radiant due to Earth's revolution around the Sun. As reference epoch we used J2000. The position of the source radiant was derived by applying a sub-pixel accuracy tracking algorithm. This algorithm was adopted from Gosse and Croquette (2002) and Otto et al. (2011). In a first step an initial position of the Geminid shower is determined by the pixel coordinate where the radiant activity map shows the highest intensity. The basic idea of the tracking algorithm is now to compute the auto-correlation function of the intensity profiles along the declination-axis and the right ascension-axis and to fit a second order polynomial to each of the auto-correlation functions to estimate the displacement from the zero lag. The displacement corresponds to two times the offset from the pixel coordinate of the initial guess. The implementation of this algorithm provides an at least one order of magnitude better measurement accuracy of the position than the actual pixel resolution of the image, which is here 2°.

In Fig. 3 the radiant position for the complete time of Geminid activity for the Andenes and Juliusruh meteor radar is shown. The shown positions are apparent source radiants and are not corrected for zenith attraction. The error bars given in Fig. 3 represent the width (extension) of the source radiant in right ascension and declination, which is defined by the applied weighting function and the measurement errors. The width of the weighting function is based on the MR interferometry, which provides an angular resolution of approximately 2° for a single specular meteor position. Therefore, these error bars cannot become smaller than 2°. The actual center position of the meteor shower shown in Fig. 3 is determined with a much higher accuracy than 1°.

However, this error is compensated by measuring a large ensemble and applying the sub-pixel accuracy fitting, which results in an error of a fraction of a degree for the centroid

Table 3. Comparison of IMO reference source radiant position to the meteor radar observations. The Juliusruh and Andenes radiant positions are not corrected for zenith attraction.

	Solar longitude	Right ascension	Declination
IMO	262.2°	112°	33°
Juliusruh	262.2°	113.1°	33.9°
Andenes	262.2°	113.6°	33.7°

position of the meteor source radiant. Another systematic error related to the interferometry are phase differences between the phase matched cables. To estimate the impact of these biases the source radiant is determined using a second meteor radar at Juliusruh. The comparison clearly indicates that both radars are in reasonable agreement and that the Geminid meteor shower position differs by less than 1°.

In Table 3 the radiant position of the Geminids is compared to the data published by the International Meteor Organization (IMO) for the peak activity period of the shower. The data can be found using the url: http://www.imo.net/calendar. However, the IMO radiant position is only given for some days during the shower, which is not sufficient for a detailed comparison. The radar data shows a small offset of about 1° in right ascension and declination for both radar locations. The meteor radar radiant position as well as the meteor head echo data is not corrected for zenith attraction (Dubyago, 1961). The contribution of the Poynting–Robertson effect (Wyatt and Whipple, 1950) is difficult to be estimated comparing the photographic observations by the IMO with the radar measurements. However, a final analysis about the reason for these discrepancies are beyond the scope of this paper.

In Fig. 4 the radiant position of the Geminids for the complete campaign period as function of solar longitude ($\lambda_\odot$) is shown. The radar measurements clearly indicate that the apparent motion of the Geminid source radiant for the right ascension angle can be well described by a linear trend model. In contrast to this behavior is the apparent motion of the declination angle with solar longitude. Before the peak of the meteor shower (solar longitude $\lambda_\odot = 262.2°$) the declination angle shows a weak linear trend towards lower angles. After the peak of the shower there is a clear breakpoint visible and the weak trend changes to a much more rapid tendency towards smaller declination angles. As a reference IMO coordinates are given for both celestial coordinates. At the moment one can only speculate about the physical reason for this behavior. A likely reason might be different ejection time and, therefore, ages of the Geminid particles, which should be checked by simulating the orbital evolution of the Geminid stream, but this will be left for future works.

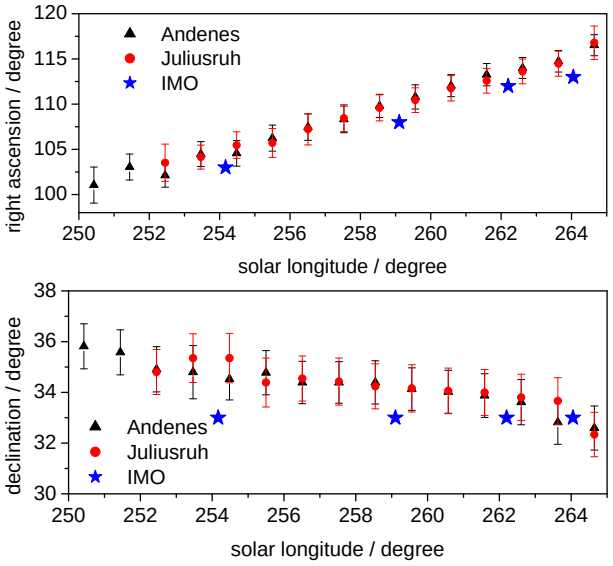

Fig. 4. Geminid radiant position for the Juliusruh and Andenes meteor radars for different solar longitudes.

3.2 Velocity measurement

There have been several different velocity determination algorithms developed to estimate the meteoroid velocity from specular meteor observations (for a summary Baggaley and Grant, 2005a,b,c; Holdsworth et al., 2007). Most of these methods make use of the typical signal characteristics due to the specular observation geometry, which is well described by a Fresnel diffraction pattern (e.g. McKinley, 1961; Baggaley, 2002; Elford, 2004). However, the achievable accuracy of the velocity estimates is fairly variable depending on the applied technique.

In the present study a pre-t_0 approach is used to estimate the meteoroid velocity. Hocking (2000) derived a method using a modified Fresnel transform to estimate the change of frequency of the Fresnel oscillations before the meteor passes the specular point along its flight path. On the basis of this approach Stober et al. (2011) estimated the meteor shower velocity of the Geminids with high accuracy from the radar data. The success rate of this method is about 5–7 %, but as shown in Stober (2009) the achievable accuracy is approximately 0.2 km s^{-1} for meteors with an signal-to-noise-ration better than 10 dB. The accuracy was estimated by performing several simulations and evaluating these computer experiments with the analysis software, which allowed comparing the measured velocity to the simulated meteoroid velocity. However, it has to be considered that this approach still assumes that the received meteor signature is completely described by a Fresnel diffraction pattern with signal attenuation caused by ambipolar diffusion. A more detailed discussion about likely biases related to this procedure is given in Baggaley and Grant (2005a,b) or Stober et al. (2011).

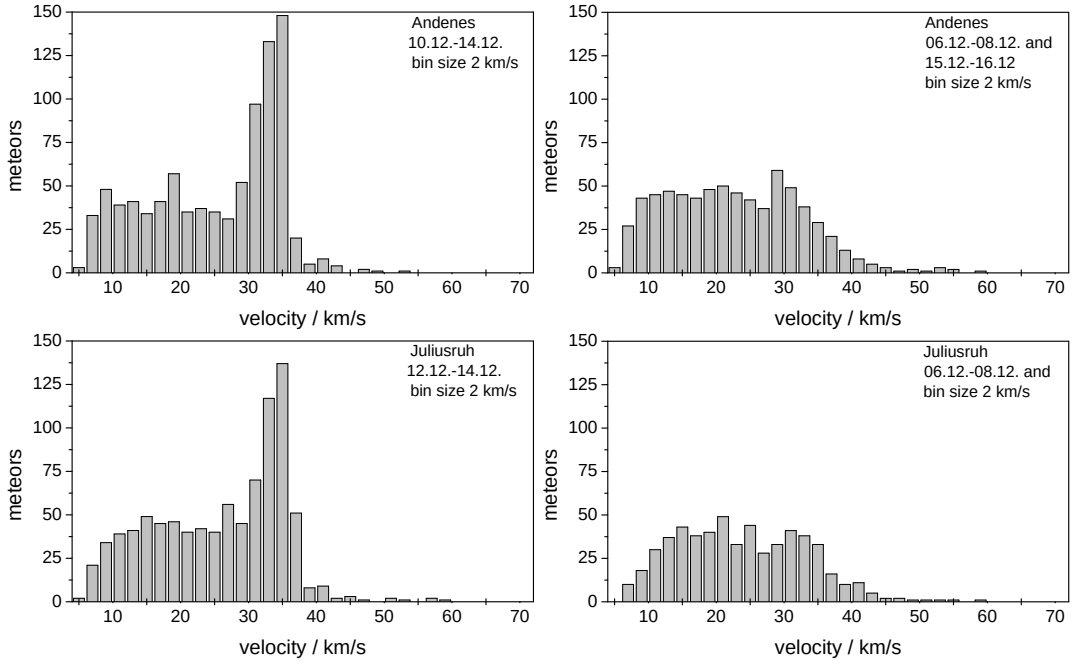

Fig. 5. Meteor velocity histograms for different periods during the ECOMA campaign for the Andenes MR (top panels) and Juliusruh MR (bottom panels).

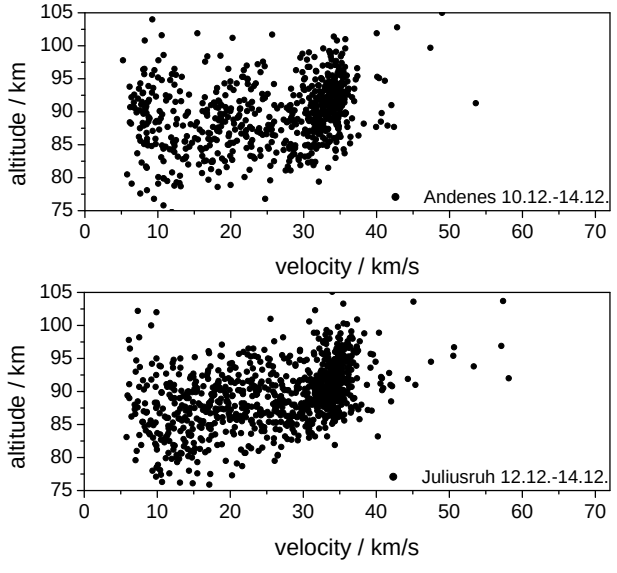

Fig. 6. Meteor altitude versus velocity distribution for the Andenes and Juliusruh MR during the peak period of the Geminid shower.

To ensure the best possible accuracy and comparability of the meteor velocity measurement an off-line analysis of the raw data was performed. In particular, the slightly lower effective PRF of the Andenes MR compared to the Juliusruh MR resulted in a reduced success rate of "good" meteor velocity measurements. Further, it is evident that due to the lower PRF the number of successful velocity determinations for meteors faster than $40\,\mathrm{km\,s^{-1}}$ is significantly decreased. This is due to the employed effective PRF, which defines the threshold for the fastest resolvable Fresnel oscillations that can be analyzed from the time series of the raw data.

In Fig. 5 the velocity histograms for different periods during the ECOMA campaign are shown for both MR. The left panels relate to the peak period of the shower and the right panels indicates the velocity distribution for the sporadic background. The different success rates for the velocity measurements between the two radars are compensated by merging different days together, which resulted in similar counts for the histograms. The detailed periods are given in the upper right corners.

The velocity of the Geminid meteor shower can be easily estimated from the histograms (left panels of Fig. 5). Both radars show a significant and relatively narrow peak around $35\,\mathrm{km\,s^{-1}}$, which is the expected velocity of a Geminid meteoroid. The width of the peak is approximately $6\,\mathrm{km\,s^{-1}}$. The sporadic meteor component shows velocities reaching from 10–$40\,\mathrm{km\,s^{-1}}$ with a peak around 20–$25\,\mathrm{km\,s^{-1}}$. Meteors with velocities above $40\,\mathrm{km\,s^{-1}}$ are under represented due to the difficulty to resolve such very fast oscillations in the raw data. Therefore, a successful velocity determination with an acceptable accuracy is hardly achieved for the fastest meteors.

However, the quality of the algorithm still allows estimating the deceleration of the meteors at least in a statistical sense. A closer inspection of the altitude vs. velocity plot shown in Fig. 6 reveals a cluster between 30–$40\,\mathrm{km\,s^{-1}}$,

which is generated by the Geminids. This cluster is a common feature at both radar locations. Obviously there is a altitude–velocity dependence, which is caused by the increasing density the deeper the meteor penetrates into the atmosphere. Meteors are already decelerated if they are detected at lower altitudes. Although this effect is small, it is an evident feature and has to be considered for estimating the upper atmospheric properties of the particle. Stober et al. (2011) demonstrated these characteristic by simulating meteors with similar upper atmosphere properties concerning mass, velocity and entry angle. Another interesting feature of the Geminids is the altitude distribution. The stream particles burn up at almost the same altitude than the typically observed sporadics.

Finally, it has to be noted that all 4 velocity histograms in Fig. 5 show at the left edge velocities below 11.1 km s^{-1}, which should be the slowest possible meteor velocity for a stable orbit around the Sun. This slower particles can either be considered as space debris or simply are caused by the meteors that are already significantly decelerated and maybe have reached the end of their flight path.

3.3 Meteor count rate and meteor fluxes

Before one can derive a meteor flux for the Geminid meteor shower, it is necessary to separate potential Geminids from the sporadic meteor background. A priori the most suitable criterion seems to be the source radiant. The position of the shower is known from the computed radiant activity maps. Therefore, it is possible to determine for every single meteor whether its GC intersects (for details see Jones and Jones, 2006) the Geminids source radiant ±5°. Every meteor fulfilling this requirement is considered as a potential Geminid. However, there is still some contamination due to sporadic meteors, which have a different velocity than the Geminids or may have a different source radiant, but their GC is close to the Geminid origin on the hemisphere.

In Fig. 7 the result of this filtering for the Andenes (top panel) and Juliusruh (bottom panel) MR is shown. The blue line represents the total observed meteor count rate. The black line indicates the sporadic meteor contribution and the red line shows the number of potential Geminid meteors. This meteor count rates were computed using a 24-h running window.

The meteor activity during the December is characterized by a weak trend of a decreasing sporadic meteor background. Superimposed to this sporadic activity are the Geminids. This meteor stream has a distinctive shape with a slowly increasing activity at the beginning (before 10 December 2010) and a significant peak period from 11 until 15 December. During the peak period the total activity of observed meteors increases by almost 50 %.

The tendency towards a decreasing sporadic meteor activity in December 2010 is also supported by Na-Lidar measurements conducted at the Alomar observatory approximately 1.7 km away from the MAARSY radar (Dunker et al., 2013). As shown in Dunker et al. (2013), this weak trend of a decreasing meteor count rate is in qualitative agreement to a decreasing Na-column density and to a reduction of the column charge density of the MSPs measured during the three rocket flights.

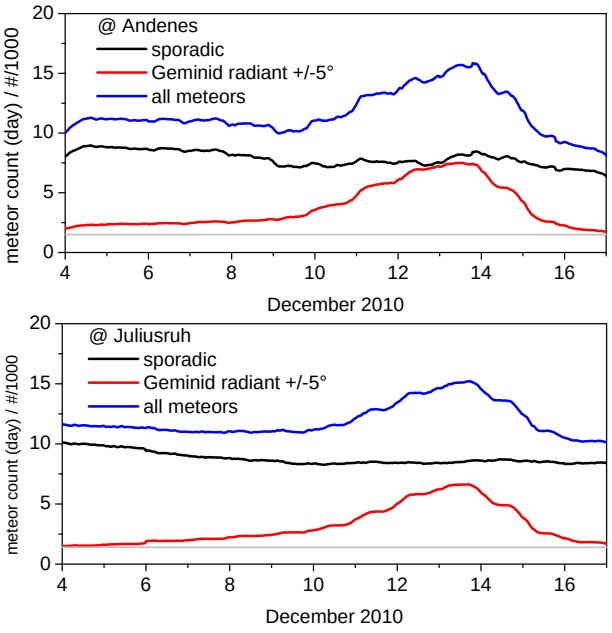

Fig. 7. Daily meteor count rate separated for sporadic activity and potential Geminids using source radiant for the Andenes and Juliusruh. The x-tickmarks indicate 00:00 UTC for each day.

The total Geminid activity is given by the red line in Fig. 7. The meteor count rate is computed using a 24 h time window, which is shifted by 30 min and centered at the time period. The time is always given in UTC. The contamination due to sporadic meteors that are unintentionally considered to be Geminids is estimated by introducing a baseline activity using the same filtering method on times before and after the shower. The baselines are given by the grey lines in Fig. 7. These background activity generated by the filtering is considered as noise. We intentionally did not subtract this baseline to demonstrate the degree of contamination of sporadics that are considered as potential Geminids.

In the following we are just focusing on the meteor activity caused by potential Geminids. In particular, the daily pattern of the observed meteor count rate will be of interest to estimate the effective radar collecting area (A). At Andenes the Geminid source radiant never descends below the horizon, which means that one can expect to observe a continuous Geminid meteor flux. In Fig. 8 the elevation of the Geminid source radiant and the observed meteor count rate are compared to demonstrate this effect. There is obviously a clear dependence between the elevation of the source radiant above the horizon and the observed meteor activity.

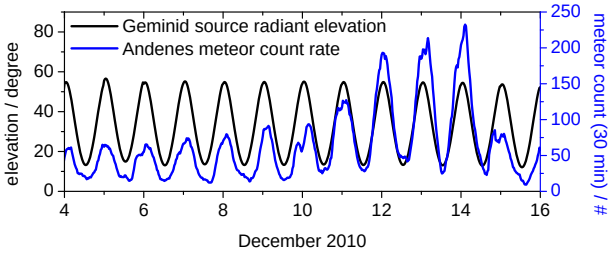

Fig. 8. Comparison of observed Geminid meteor activity with the elevation of the Geminid source radiant above the horizon. The x-tickmarks indicate 00:00 UTC for each day.

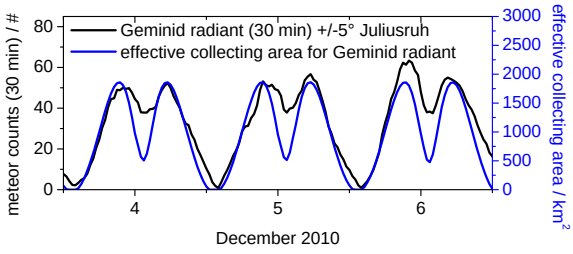

Fig. 9. Comparison of effective radar collecting area and observed meteor count rate for the Juliusruh MR. The x-tickmarks indicate 00:00 UTC for each day.

The reason for this diurnal pattern at Andenes is given by the dependence of the variation of the effective radar collecting area during the day.

First estimates of the effective radar collecting area go back to Kaiser (1960). In principle the effective radar collecting area is described by a vertical trail length and the line integral of the echo line weighted with the antenna gain pattern.

$$A(\chi, s) = \int (G(\chi) \cdot \cos(\chi))^{s-1} \, H(s) dl \qquad (2)$$

Here χ is the zenith angle, H is the vertical trail length (Fleming et al., 1993; Brown and Jones, 1995; Brown et al., 1998), G is the antenna gain, s is the cumulative mass index and dl is an infinitesimal short piece along the echo line. Assuming a cumulative mass index of $s = 2$ (Blaauw et al., 2011a), a model for the vertical trail length $H(s)$ (Fleming et al., 1993; Brown et al., 1998) and solving the equation numerically leads to an estimate of the effective radar collecting area for a given meteor radiant with a zenith distance χ. Considering the empirical equation in Brown et al. (1998) results in a vertical trail length of approximately 4.8 km assuming $s = 2$. In fact, the Geminids tend to have a cumulative mass index smaller than the sporadic meteor population of $s = 1.7$ (Blaauw et al., 2011b), which could lead to an approximately two times larger effective collecting area integrating over all possible elevation angles. The assumption of $s = 2$ is for the comparison with the sporadic meteor population a bit more

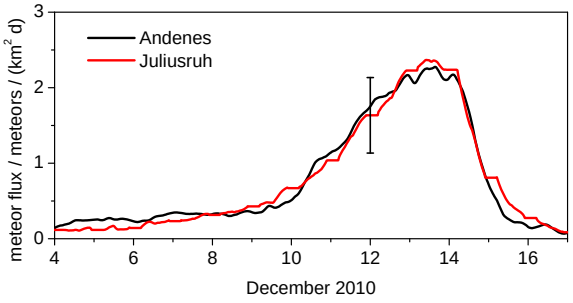

Fig. 10. Comparison of absolute fluxes for the Andenes and Juliusruh MR after the subtraction of the baseline due to sporadic background activity close to the Geminid source radiant. The x-tickmarks indicate 00:00 UTC for each day.

exaggerating and tends to overestimate the flux caused by the Geminids.

The validity of the equation is checked by comparing the 30 min meteor count rate with the effective collecting area using the elevation of the Geminid source radiant above the horizon for each time interval. To evaluate the effective collecting area equation and its properties, we focused on the Juliusruh MR to demonstrate how the effective collecting area changes with time.

Figure 9 compares both quantities. The effective collecting area as well as the meteor activity have two prominent minima in the time series. The meteor count rate was computed using a 4-h running window shifted by 30 min. We also tried to estimate the meteor count rate using shorter time windows of 1 h and 2 h, but it turned out that the data becomes too "noisy" to still perform this comparison. The effective collecting area was computed always for the center time of each period, which explains some of the observable differences. However, the minimum that occurs every day around 12:00 UT is related to the time when the Geminid source radiant is below the horizon or has only a very low elevation angle. The second minimum corresponds to times when the source radiant reaches its highest elevation angle, which is during the early morning hours UT. However, the meteor count rate and the effective meteor collecting area are in reasonable agreement and both show a similar behavior, which demonstrates that it is possible to relate variations of the observed meteor count rate with a variation of the effective meteor collecting area.

Finally, an attempt is made to derive absolute meteor fluxes using the computed effective radar collecting area. To avoid any difficulties with singularities due to an effective collecting area close to zero only a daily mean area is considered, ignoring any times where the Geminid source radiant is below or close to the horizon. In Fig. 10 the absolute meteor fluxes for the Andenes and Juliusruh MR are shown. Both radars observe the same meteor flux, which reaches a peak intensity of 2.5 meteors km^{-2} d after subtraction of the baseline activity due to the sporadics. However, the contamination due

to sporadic meteors is taken from the meteor count rate and is already subtracted. Another important error source is the variation of the cumulative mass index s, which has a direct impact on the effective collecting area. The error bar shown at 12 December is representative for the analysis and both radars and was computed by an variation of s in the computation of the effective collecting area. Due to the unknown uncertainty of the vertical trail length, this error was not included in the computation of the error bar.

The absolute meteor flux including all meteors during the time interval reached a value of 6 meteors km^{-2} d at both radar locations. This means that 40 % of the observed meteors originated from the Geminid meteor shower. However, one essential point deriving absolute meteor fluxes is to estimate the particle size range of the observed particles. This particle size range was determined by applying the method as described in Stober et al. (2011) using a single body meteor ablation model. In a first step the meteoroid mass is inferred at the specular point by solving the equations of single body meteor ablation using all the measured parameters (e.g. electron line density, altitude, entry angle, velocity). By solving the model equations we compute the meteoroid deceleration, the meteoroid surface temperature and the meteoroid particle mass at this stage of its flight path. The upper atmospheric properties of the meteors are inferred by performing a backward integration. The Geminid upper atmospheric meteoroid mass was in the range of 3×10^{-3}–10^{-5} g at both radar sites. The 10^{-5} g represents the lower mass limit to be detected by the system for Geminid entry velocity.

Estimating the meteor flux and referring this flux to the complete Earth surface as reference area allows comparing the results with the mass input functions of Ceplecha et al. (1998) and Rietmeijer (2000). The estimated MR meteor flux for particles with mass $m = 1^{-4}$ g reaches an almost one order of magnitude higher mass flux than the prediction of Ceplecha et al. (1998), but remains still 2 orders of magnitude smaller than the mass flux from Rietmeijer (2000) or Love and Brownlee (1993). The MR indicates at least for the investigated mass range that the curve of Ceplecha et al. (1998) tends to under estimate the meteoric mass input at this specific particle size. However, the estimated MR fluxes are still below the meteoric mass input that can be inferred for this particle size range using the curve of Rietmeijer (2000). Considering an even smaller mass distribution index of $s = 1.7$ (Blaauw et al., 2011b) for the Geminids would even further decrease the observed meteor flux by a factor of 2 to smaller values, which still could not explain the orders of magnitude difference to the reference curves.

To understand the differences between these meteor flux estimates, one has to consider the different methods how these fluxes are derived. The most useful quantification of the meteor influx is to estimate how many meteors exist at a certain mass range before these meteoroids enter Earth's atmosphere and undergo a likely mass loss. The mass input from Love and Brownlee (1993) is based on such free space meteoroids, but requires assuming a mean impact velocity of particles. The curve from Rietmeijer (2000) has its origin from meteorites collected on earth's surface, which likely did undergo some ablation. Ceplecha et al. (1998) inferred the meteor influx using various methods. The difficulty in comparing all these curves is how the meteors ablate and how much meteoric material is ablated. It is rather complex to estimate the upper atmospheric properties (e.g. mass) of a meteorite and requires some assumption of the ablation process.

The mass range covered by the MR observations are hardly accessible by other methods. In addition, the radar measurements provide a direct insight into the meteor ablation physics, which is a key element to understand the meteoric mass deposit in the MLT or to estimate the upper atmospheric meteoroid properties. One issue that is not completely solved yet is the ionization efficiency (Jones, 1997), which relates the amount of ablated meteoric matter to the number of electrons/ions in the meteor trail or plasma around a meteor head echo.

Apart from the absolute meteor flux estimates of the Geminid meteor stream, we also compared the sporadic meteor count rate, the sounding rocket measurements of negatively charged meteoric smoke particles (Rapp et al., 2012) and Na-column density observations (Dunker et al., 2013). Dunker et al. (2013) showed that the weak trend of a decreasing sporadic meteor activity seen by the MR is at least in qualitative agreement with a decreasing Na-column density in December 2010 and a decrease of the MSPs charge column density comparing the three sounding rocket flights.

According to Dunker et al. (2013), the Na-column density can be used to infer the total meteoric mass input, which is mainly given by particles in the mass range between 10^{-6}–10^{-4} g. Further, Rapp et al. (2012) showed that the MSP properties are rather determined by the sporadic meteor flux in these particle size range than by meteors in the mass range of 10^{-4}–10^{-3} g. In so far it is interesting that the sporadic meteor activity observed by the MR indicates this reasonable qualitative agreement to the Na-column density and MSP measurements, which are related to the total meteoric mass influx.

This further indicates that, at least in this comparison, the Geminid meteor shower can be ruled out to be of significant relevance for the MSP properties or to deposit a significant amount of meteoric material in the MLT region. However, as suggested by von Zahn (2005) there is a need to measure the meteor influx for particles in the size range between 10^{-6}–10^{-4} g, which should be possible by observing meteor head echoes.

4 Meteor head echoes

Over the past decade meteor head echo observations using High-Power Large-Aperture HPLA radars have become a vital field of research (e.g. Mathews et al., 2001; Chau

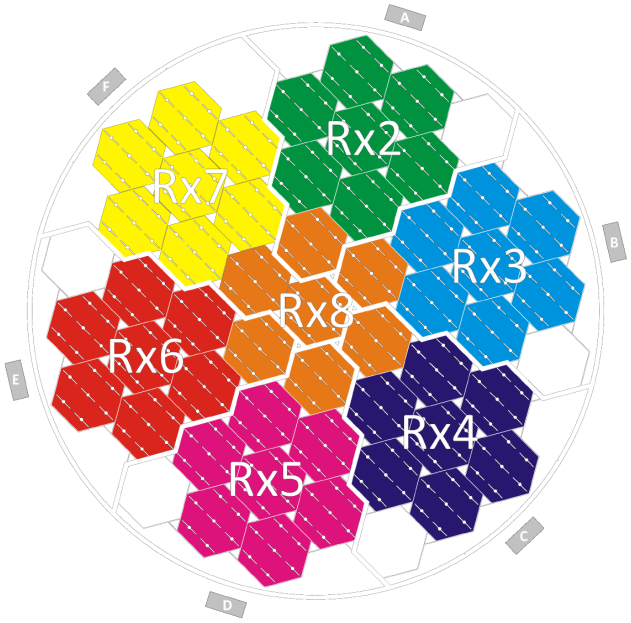

Fig. 11. The receiver configuration of MAARSY during the ECOMA sounding rocket campaign.

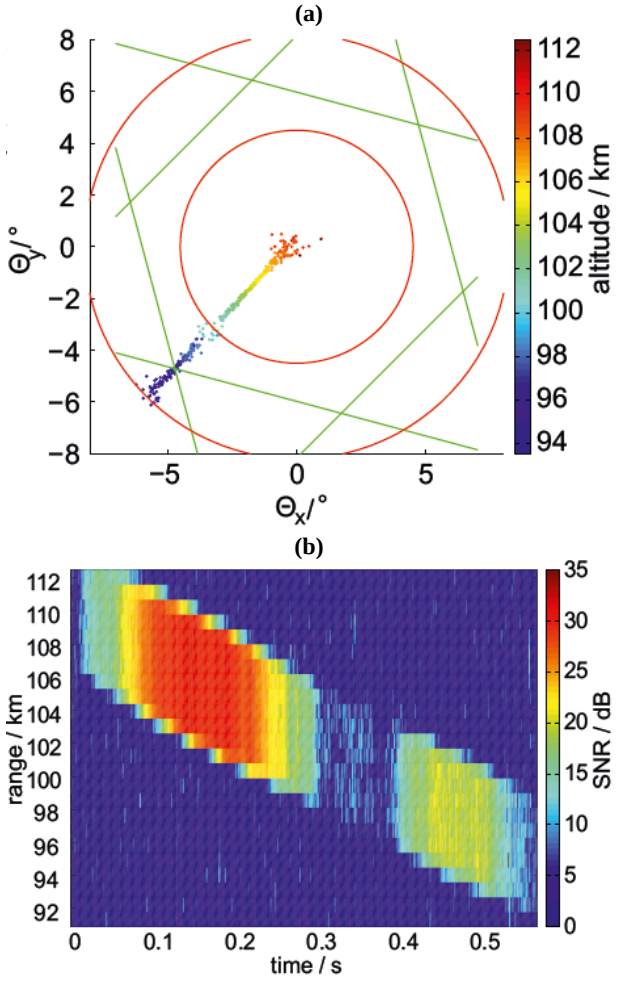

Fig. 12. (a) Projection of a meteor head echo in the 2-D plane after an interferometric analysis. **(b)** Range-time SNR plot of the same meteor head echo.

and Woodman, 2004; Pellinen-Wannberg, 2004; Chau et al., 2007; Janches et al., 2009; Sparks et al., 2010; Kero et al., 2011). However, meteor head echo experiments are often conducted as short campaigns and contain usually only a few hours/days of observations, which makes it hard to derive a meteor climatology of the sporadic meteor background or to investigate meteor showers lasting several days.

Among the HPLA radars, phased arrays have become a powerful tool to investigate this type of echo due to the interferometric capabilities of these systems (Jicarmarca, PFISR, MU radar), which permits the determination of the meteoroid trajectory within the beam volume (e.g. Chau and Woodman, 2004; Sparks et al., 2010; Kero et al., 2011). The meteor head echo results presented from here on are based on MAARSY measurements using 8 receiver channels. One channel was assigned to record the signal of the complete available array and is used to detect head echo signatures. The remaining seven channels were connected to sub-arrays each of which consisted of 49 antennas. The receiver configuration is shown in Fig. 11. The phase difference between the phase matched cables was approximately 1° (Latteck et al., 2012b).

The MAARSY meteor head echo experiment was conducted continuously, but interleaved with several other experiments monitoring atmospheric winds and polar mesospheric winter echoes. This led to an total observation time of 28 h, which were distributed in such a way that it is still possible to measure the daily pattern of the meteor activity as well as to cover the complete period of the Geminid activity.

For the analysis of the meteor head data an automated software tool was developed. In a first step the cosmic background noise level for all height gates and the complete raw data sample (one raw data sample contained 12 s) was determined. On the basis of this background power level a SNR value for each raw data point was computed. This SNR time series was than searched for enhanced SNR areas to detect probable head echoes. If a likely head echo was found a similar procedure was applied to the receiver channels 2–8 and an interferometric analysis was performed.

In Fig. 12a an example of a detected head echo is shown. The red lines in this panel denote minima of the antenna radiation pattern (Latteck et al., 2012b). The green lines represent ambiguity areas due to the given baseline length of 28 m. These ambiguity areas are computed in analogy to Sparks et al. (2010). The trajectory of the head echo started right in the center of the main beam and moved outwards, disappeared and showed up again in the first side lobe. The color code indicates the altitude of the meteoroid according to the interferometric analysis. In this case it is easy to remove the phase ambiguity by simply unwrapping the signal

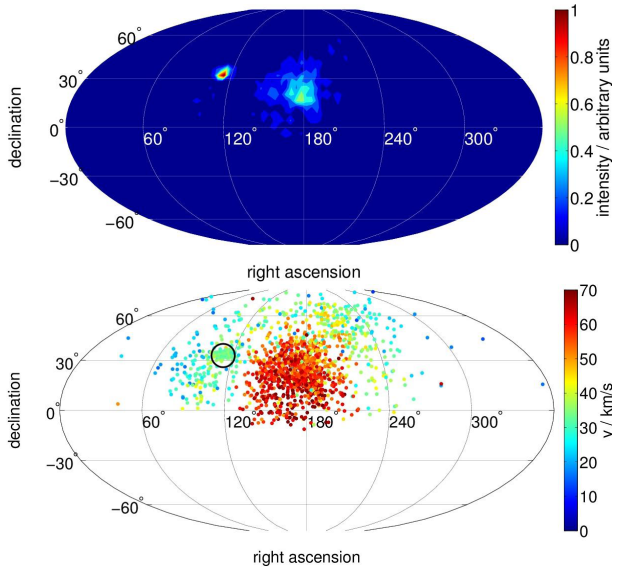

Fig. 13. Top: MAARSY radiant intensity plot normalized to Geminid source radiant. Bottom: head echo radiant distribution with color coded velocity.

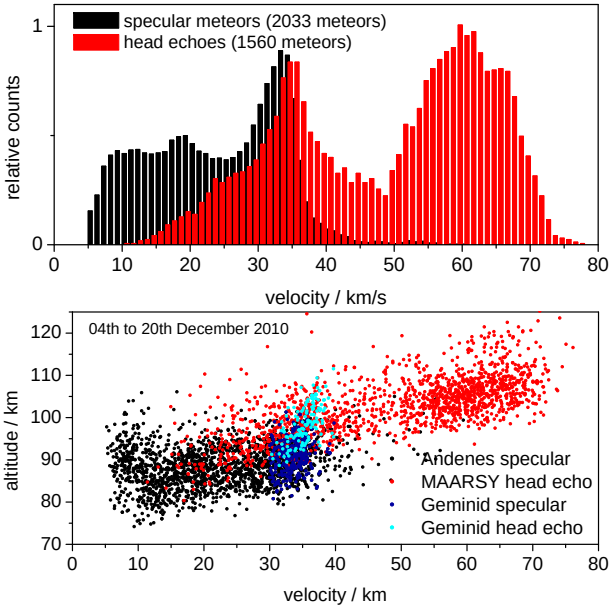

Fig. 14. Top: Meteor head echo velocity histograms for the meteor head echo and specular meteor observations. Bottom: Altitude versus velocity distribution during the ECOMA sounding rocket campaign.

considering the range where the head echo occurred. The SNR plot (Fig. 12b) also indicates the minimum of the radiation pattern. The head echo SNR decreases between 0.28 and 0.38 s and appears again in the side lobe. However, there are only a few events that occur both in the main beam and in the side lobe.

Further, we computed the errors of the interferometric analysis for each meteor. We only accepted meteor head echoes with a vector velocity error smaller than $\pm 2\,\mathrm{km\,s^{-1}}$, which was achieved in 99.7 % of all analyzed meteor events. 91 % of all azimuth angles and 97 % of all elevation angles were determined with an accuracy better than 2°. The largest error we found in the analysis was 3°. However, typically the vector velocity was determined to better than $1\,\mathrm{km\,s^{-1}}$ and the average angular error was smaller than 1° in both angles. The accuracy of the head echo trajectories are good enough to separate Geminid meteors from the sporadic background due to their entry velocity and source radiant with a better precision than for the MR.

The complete period was analyzed using an automated routine. In total 1560 meteor head echoes were found. For all of these head echoes it was possible to measure a radial velocity and to determine a reliable trajectory as well as the vector velocity. In Fig. 13 two source radiant maps of all head echoes are shown. The top panel indicates an arbitrary intensity similar to the radiant maps derived from the MR at Andenes. A common feature of head echo and MR radiant maps is that the Geminid source radiant is still dominating. The source radiant of the Geminids was determined to have a right ascension of $\alpha = 112.5°$ and a declination of $\delta = 32.5°$ for the peak activity period (reference epoch J2000). In contrast to the MR radiant activity maps there is a second pronounced activity region mainly caused by the sporadic meteor background. In particular, the north apex source seems to provide a significant contribution to the observed sporadic meteors. The main reason for this difference of the radiant activity maps is given by the observed velocities (see Fig. 14). The bottom panel shows the source radiant for each head echo. The absolute value of the vector velocity is given as color code. The Geminid source radiant is highlighted by a black circle. Inside the black circle almost all meteors show velocities close $35\,\mathrm{km\,s^{-1}}$.

To separate potential Geminid meteor head echoes from the sporadic meteor background, we considered all meteors within 10° in right ascension and 5° in declination of the Geminid source radiant and a vector velocity between $30–40\,\mathrm{km\,s^{-1}}$ as Geminid meteoroids. By applying this filter we were able to identify 118 Geminid meteoroids during the complete sounding rocket campaign period. Compared to the specular radars the ratio between sporadic meteors and Geminid meteors has significantly decreased. However, there are biases related to the head echo observations such as the mass-velocity selection effect (Close et al., 2006) and the altitude cut-off (Westman et al., 2004). The presented results permit deriving a tendency about the cumulative mass index. Our measurements of the Geminid meteor shower support that the stream contains more mass in the larger particles (specular meteors) than in the smaller meteoroids (head echoes). This is consistent with Blaauw et al. (2011b) and implies a cumulative mass index smaller than $s = 2$. Based on the present

analysis it is not yet possible to quantify the value of s and to derive a robust estimate of the cumulative mass index covering the mass range from 3×10^{-3}–10^{-7} g. This requires a more detailed analysis and to determine the mass/size of meteor head echoes.

There are several unsolved difficulties that have to be taken into account before one gets reliable meteor head echo mass estimates. In particular, the meteor trajectory through the radar volume has to be determined with the highest possible accuracy to avoid errors estimating the RCS and deceleration of the meteoroid, which will directly lead to huge uncertainties of the scattering or dynamical meteor mass (Close et al., 2006). Measuring all of these meteoroid quantities permits solving the equations of single body meteor ablation model and computing much more realistic upper atmospheric meteoroid properties similar to the method given in Stober et al. (2011).

In Fig. 14 a comparison of the measured velocity distributions is shown. Both distributions are normalized to account for the different number of events. The red columns represent the velocity distribution of the head echoes and the black columns belong to the Andenes MR. The red histogram bars are shifted by 0.5 km s^{-1} to higher velocities to avoid an overlapping of both histogram data sets. The red histogram clearly shows a double peak structure. There is a rather broad peak around 60 km s^{-1}, which belongs to the sporadic meteor background. These fast meteors mainly have their origin in the north apex source and revolve around the Sun on retrograde orbits. The second peak at 35 km s^{-1} belongs to the Geminid meteor shower.

Comparing the specular meteor (black bars) with the meteor head (red bars) observations indicates the well-known effect that the systems seem to observe different parts of the total meteor population. However, one should keep in mind that the specular velocity distribution is biased to good signal-to-noise-ratio leading to an under-representation of fast meteors (> 40 km s^{-1}). It is much harder to resolve the fast Fresnel oscillations of the faster meteors with the employed effective PRF. On the other side are the head echo measurements biased due to a cut off altitude given by the required plasma density to observe the head echo (Westman et al., 2004; Pellinen-Wannberg et al., 2004). The efficiency of the plasma production depends on velocity and mass, which makes it harder for meteoroids traveling at "slower" velocities (< 30 km s^{-1}) to reach the critical plasma density to be detected by the HPLA.

Concerning the Geminid meteor shower both velocity histograms show a peak around 35 km s^{-1}. In particular the peak positions are within 1 km s^{-1} and hence are in reasonably good agreement. A closer look at the Geminid peak areas show a shift between both measurements. This offset is explainable considering the altitude of observation of both techniques. An altitude vs. velocity plot is shown in Fig. 14 (bottom panel). This plot indicates that there is a systematic 10 km altitude difference between both radar methods. The origin of this altitude difference is likely caused by the different particle sizes of the observed meteoroids, but also contains effects caused by the radar method. In particular, above 100 km the decay of the meteor trails becomes so fast that these meteors are hardly detected by specular radars. The plot shows a clear tendency that faster meteors burn up at higher altitudes than slower meteors. Further, it is evident that the bulk of the head echoes is detected at altitudes between 95–110 km. The Geminid meteor shower is still seen in this plot as a dense area around 35 km s^{-1}. All potential Geminid meteors are indicated as blue (specular) and cyan (head echoes) dots. Similar to the specular observations one can identify the deceleration of the meteors with the altitude. Obviously, the difference between the peak structures of the Geminid in the velocity histograms is created by the difference of the detection altitude.

There is also a relevant group of objects showing velocities below 11.1 km s^{-1}, which is the escape velocity from Earth's gravitational field. These objects are likely related to space debris or already decelerated meteors. The reason for the slightly increased altitudes compared to the meteor population faster than 11.1 km s^{-1} is not yet understood.

Taking this altitude difference into account leads to an even better agreement of the velocity measurements for both observation techniques. In particular, the effect of stronger deceleration the deeper the meteoroid penetrates into the atmosphere is visible comparing the specular and head echo observations. However, from simulations it is known that the deceleration remains small until the meteoroid comes close to its complete vaporization (Pellinen-Wannberg et al., 2004) (termination of flight path).

The major difference between the specular and head echo meteor observations concerning the Geminids is the relative contribution of the stream meteors to the total observed meteor flux. The relative number of Geminid meteors is about 7 % of all detected particles with MAARSY, which is significantly less than for the MR reaching a relative contribution of about 40 %.

5 Conclusions

During the ECOMA sounding rocket campaign, radar measurements to monitor the Geminid meteor shower were performed. Therefore, two MR at polar and mid-latitudes were used. The MR observations were supplemented by MAARSY head echo measurements.

The continuous specular radar observations provide an ideal tool to analyze the apparent radiant motion of the Geminid meteor shower over a period of almost two weeks. The accuracy of the measured radiant position indicates only a small offset between the Juliusruh and Andenes MR. Comparing these radiant positions to those of the IMO, indicates a tendency of the MR to 1° higher declination angles at the beginning of the shower. The radiant position of meteor head

echo observations is somewhere in between the IMO reference and the MR.

The MR velocity measurement shows for Andenes and Juliusruh a clear peak structure around 35 km s^{-1} and a one sigma width of $\pm$3 km s^{-1} for times with a significant Geminid meteor activity (10 to 14 December). The shape of the histogram combined with the altitude distribution of the Geminids shows a stronger deceleration of the shower meteors the deeper they are penetrating into the atmosphere. This deceleration has to be taken into account before one can determine a reliable "top of the atmosphere" velocity of the meteoroids. The deceleration with altitude also explains why the distribution of the Geminid peak in the velocity histogram is slightly asymmetric and tends to slower velocities.

On the basis of the radiant activity maps and the tracked radiant position of the Geminid meteor shower, we tried to estimate the contribution of this stream to the complete meteor flux in the observed size/mass range. Therefore, all meteors with a likely source radiant close to the Geminids were filtered. The contamination due to sporadics and ambiguity effects introduced by the statistical method are estimated by monitoring times before and after the shower. The relative contribution indicates a small difference between Andenes (almost 50 %) and Juluisruh (almost 44 %), which is mainly caused by geometrical effects. At Juliusruh the Geminid source radiant drops below the horizon, while at Andenes it remains above for the complete day.

Using Kaiser's theory (Kaiser, 1960) to estimate the effective collecting area for both specular radar locations permits computing absolute meteor fluxes for the observed particle size/mass range. The mean daily meteor fluxes do not show any significant difference between the two radar locations. The Geminids reach during their peak activity a relative contribution of 40 % to the total observed meteor flux in the particle size range of 3×10^{-3}–10^{-5} g.

The first head echo observations with MAARSY provided an ideal opportunity to test its interferometric abilities to measure meteor trajectories. The collected data of 28 h of observation during the ECOMA sounding rocket campaign is a unique head echo data set to investigate the Geminid meteor shower. From these measurements we were able to identify 118 Geminid meteors out of the 1560 head echoes. The radiant position of the Geminid head echoes is in reasonable agreement to the IMO reference and the MR radiant position.

The vector velocity of the meteoroids was determined with acceptable accuracy using the interferometric abilities of MAARSY. The combination of all "anemone" substructures increased the accuracy of the measured trajectories and provided a first estimate to check the different receiver channels for phase offsets. The initial results showed an agreement within $\pm 1°$.

The vector velocity measurements as well as the altitude distribution are in reasonable agreement with the Andenes MR observations. The vector velocity histogram of the Geminid meteor peak indicates a weak shift towards fast velocities. This is explained by the different detection altitudes and the stronger deceleration of the particles the deeper they penetrate into the atmosphere. This is also confirmed by comparing the altitude distribution between both techniques. A scatter plot of the velocity vs. altitude shows a denser area around 35 km s^{-1} belonging to the Geminid shower. In the overlap region between the head echo and the MR data both measurements are in excellent agreement.

The head echo results presented in this work are initial and further efforts are required to estimate the corresponding meteor fluxes, the daily variation of the meteor activity and to improve our automated routine to detect meteor head echoes.

The comparison of the MSP sounding rocket measurements and the Na-column density observations demonstrate the potential of meteor radars to infer the total meteoric mass deposit at the MLT. The reasonable agreement should be used to constrain the meteoric mass input for the observed particle sizes. In particular, the specular and head echo observations should be combined to derive a reliable cumulative mass index for the sporadic meteor population covering the particle size range from about 10^{-6}–10^{-2} g.

Acknowledgements. The support of the Andøya Rocket Range is acknowledged. We thank Freddy Galindo for his valuable discussions about the interferometric analysis of the meteor head echo data. The authors also thank Takuji Nakamura for helpful discussions about meteor head echo experiments with MU radar. The authors want to thank the two reviewers for investing their time and the valuable discussion improving this manuscript.

Guest Editor U.-P. Hoppe thanks M. Tsutsumi and one anonymous referee for their help in evaluating this paper.

References

Baggaley, W.: Radar Observations, in: Meteors in the Earth's Atmosphere, Cambridge University Press, 2002.

Baggaley, W. and Grant, J.: Techniques for measuring radar meteor speeds, Earth Moon and Planets, 95, 601–615, 2005a.

Baggaley, W. and Grant, J.: Radar measurements of meteoroid decelerations, Earth Moon and Planets, 95, 647–654, 2005b.

Baggaley, W. and Grant, J.: Radar measurements of macro fragmentation in meteoroids, Earth Moon and Planets, 95, 655–662, 2005c.

Baggaley, W., Bennett, R., Steel, D., and Taylor, A.: The advanced Meteor Orbit Radar Facility: AMOR, Q. J. R. Astr. Soc., 35, 293–320, 1994.

Baggaley, W., Bennett, R., and Taylor, A.: Radar meteor atmospheric speeds determined from echo profile measurements, Planet. Space Sci., 45, 577–583, 1997.

Blaauw, R. C., Campbell-Brown, M. D., and Weryk, R. J.: Mass distribution indices of sporadic meteors using radar data, Mon. Not. R. Astron. Soc., 412, 2033–2039, doi:10.1111/j.1365-2966.2010.18038.x, 2011a.

Blaauw, R. C., Campbell-Brown, M. D., and Weryk, R. J.: A meteoroid stream survey using the Canadian Meteor Orbit Radar – III. Mass distribution indices of six major meteor showers,

Mon. Not. R. Astron. Soc., 414, 3322–3329, doi:10.1111/j.1365-2966.2011.18633.x, 2011b.

Brown, P. and Jones, J.: A Determination of the Strengths of the Sporadic Radio-Meteor Sources, Earth, Moon, and Planets, 68, 223–245, 1995.

Brown, P., Hocking, W. K., Jones, J., and Rendte, J.: Observations of the Geminids and Quadrantids using a stratosphere-troposphere radar, Mon. Not. R. Astron. Soc., 295, 847–859, 1998.

Campbell-Brown, M. and Jones, J.: Annual variation of sporadic radar meteor rates, Mon. Not. R. Astron. Soc., 367, 709–716, 2006.

Ceplecha, Z., Borovicka, J., Elford, W., Revelle, D., Hawkes, R., Porubcan, V., and Simek, M.: Meteor phenomena and bodies, Space Sci. Rev., 84, 327–471, 1998.

Chau, J. L. and Woodman, R. F.: Observations of meteor-head echoes using the Jicamarca 50 MHz radar in interferometer mode, Atmos. Chem. Phys., 4, 511–521, doi:10.5194/acp-4-511-2004, 2004.

Chau, J. L., Woodman, R. F., and Galindo, F.: Sporadic meteor sources as observed by the Jicamarca high-power large-aperture VHF radar, Icarus, 188, 162–174, 2007.

Close, S., Brown, P., Campbell-Brown, M., Oppenheim, M., and Colestock, P.: Meteor head echo radar data: Mass-velocity selection effects, Icarus, 186, 547–556, 2006.

Dubyago, A.: The determination of orbits, New York, Macmillan, 1961.

Dudnik, B. S., Kashcheev, B. L., Lagutin, M. F., and Lysenko, I. A.: The Velocity of Meteors of the Geminid Shower, Soviet Astronomy, 3, 143–146, 1959.

Dunker, T., Hoppe, U.-P., Stober, G., and Rapp, M.: Development of the mesospheric Na layer at 69° N during the Geminids meteor shower 2010, Ann. Geophys., 31, 61–73, doi:10.5194/angeo-31-61-2013, 2013.

Elford, W. G.: Radar observations of meteor trails, and their interpretation using Fresnel holography: a new tool in meteor science, Atmos. Chem. Phys., 4, 911–921, doi:10.5194/acp-4-911-2004, 2004.

Fleming, D., Hawkes, R., and Jones, J.: Light curves of fiant television meteors, Astronomical Institute, Slovak Academy of Sciences, Bratislava, 1993.

Gosse, C. and Croquette, V.: Magnetic tweezers: Micromanipulation and force measurement at the molecular level, Biophysical Journal, 82, 3314–3329, 2002.

Hocking, W.: Real-time meteor entrance speed determinations made with interferometric meteor radars, Radio Sci., 35, 1205–1220, 2000.

Hocking, W., Fuller, B., and Vandepeer, B.: Real-time determination of meteor-related parameters utilizing modern digital technology, J. Atmos. Solar-Terr. Phys., 63, 155–169, 2001.

Holdsworth, D. A., Elford, W. G., Vincent, R. A., Reid, I. M., Murphy, D. J., and Singer, W.: All-sky interferometric meteor radar meteoroid speed estimation using the Fresnel transform, Ann. Geophys., 25, 385–398, doi:10.5194/angeo-25-385-2007, 2007.

Janches, D., Dyrud, L., Broadley, S., and Plane, J.: First observation of micrometeoroid differential ablation in the atmosphere, Geophys. Res. Lett., 36, 6, doi:10.1029/2009GL037389, 2009.

Jones, W.: Theoretical and observational determinations of the ionization coefficient of meteors, Mon. Not. R. Astron. Soc., 288, 995–1003, 1997.

Jones, J. and Jones, W.: Meteor radiant activity mapping using single-station radar observations, Mon. Not. R. Astron. Soc., 367, 1050–1056, 2006.

Jones, J. and Morton, J.: High-resolution radar studies of the Geminid meteor shower, Mon. Not. R. Astr. Soc., 200, 281–291, 1982.

Jones, J., Brown, P., Ellis, K., Webster, A., Campbell-Brown, M., Krzemenski, Z., and Weryk, R.: The Canadian Meteor Orbit Radar: system overview and preliminary results, Planet. Space Sci., 53, 413–421, doi:10.1016/j.pss.2004.11.002, 2005.

Kaiser, T.: The determination of the incident flux of radio-meteors, Mon. Not. R. Astron. Soc., 121, 284–298, 1960.

Kero, J., Szasz, C., Nakamura, T., Meisel, D. D., Ueda, M., Fujiwara, Y., Terasawa, T., Miyamoto, H., and Nishimura, K.: First results from the 2009–2010 MU radar head echo observation programme for sporadic and shower meteors: the Orionids 2009, Mon. Not. R. Astron. Soc., 416, 2550–2559, 2011.

Latteck, R., Singer, W., Morris, R. J., Hocking, W. K., Murphy, D. J., Holdsworth, D. A., and Swarnalingam, N.: Similarities and differences in polar mesosphere summer echoes observed in the Arctic and Antarctica, Ann. Geophys., 26, 2795–2806, doi:10.5194/angeo-26-2795-2008, 2008.

Latteck, R., Singer, W., Rapp, M., Renkwitz, T., and Stober, G.: Horizontally resolved structure of radar backscatter from polar mesospheric layers, Adv. Radio Sci., 10, 1–6, 2012a, http://www.adv-radio-sci.net/10/1/2012/.

Latteck, R., Singer, W., Rapp, M., Vandepeer, B., Renkwitz, T., Zecha, M., and Stober, G.: MAARSY: The new MST radar on Andøya-System description and first results, Radio Sci., 47, 1, doi:10.1029/2011RS004775, 2012b.

Love, S. G. and Brownlee, D. E.: A Direct Measurement of the Terrestrial Mass Accretion Rate of Cosmic Dust, Science, 262, 550–553, 1993.

Mathews, J. D., Janches, D., Meisel, D. D., and Zhou, Q.-H.: The micrometeoroid mass flux into the upper atmosphere: Arecibo results and a comparison with prior estimates, Geophys. Res. Lett., 28, 1929–1932, 2001.

McKinley, D.: Meteor Science and Engineering, McGraw-Hill, Toronto, 1961.

Megner, L., Rapp, M., and Gumbel, J.: Distribution of meteoric smoke – sensitivity to microphysical properties and atmospheric conditions, Atmos. Chem. Phys., 6, 4415–4426, doi:10.5194/acp-6-4415-2006, 2006.

Megner, L., Siskind, D. E., Rapp, M., and Gumbel, J.: Global and temporal distribution of meteoric smoke: A two-dimensional study, J. Geophys. Res., 113, D03202, doi:10.1029/2007JD009054, 2008.

Nesvorný, D., Jenniskens, P., Levison, H. F., Bottke, W. F., Vokrouhlický, D., and Gounelle, M.: Cometary origin of the Zodiacal cloud and carbonaceous micrometeorites. Implications for hot debris disks, The Astrophysical Journal, 713, 816–836, doi:10.1088/0004-637X/713/2/816, 2010.

Öpik, E.: Physics of Meteor Flight in the Atmosphere, Interscience Publisher, Inc., New York, 1958.

Otto, O., Gormall, J., Stober, G., Czerwinski, F., Seidel, R., and Keyser, U. F.: High-speed video-based tracking of optically trapped colloids, Journal of Optics, 13, 044011, 2011.

Pellinen-Wannberg, A.: The EISCAT meteor-head method – a review and recent observations, Atmos. Chem. Phys., 4, 649–655,

doi:10.5194/acp-4-649-2004, 2004.

Pellinen-Wannberg, A., Murad, E., Wannberg, G., and Westman, A.: The Hyperthermal Ionization and high absolute meteor velocities observed with HPLA radar, Earth, Moon, and Planets, 95, 627–632, 2004.

Rapp, M., Plane, J. M. C., Strelnikov, B., Stober, G., Ernst, S., Hedin, J., Friedrich, M., and Hoppe, U.-P.: In situ observations of meteor smoke particles (MSP) during the Geminids 2010: constraints on MSP size, work function and composition, Ann. Geophys., 30, 1661–1673, doi:10.5194/angeo-30-1661-2012, 2012.

Rietmeijer, F.: Interrelationships among meteoric metals, meteors, interplanetary dust, micrometeorites, and meteorites, Meteoritics and Planetary Science, 35, 1025–1041, 2000.

Singer, W., Bremer, J., Hocking, W., Weiss, J., Latteck, R., and Zecha, M.: Temperature and wind tides around the summer mesopause at middle and Arctic latitudes, Adv. Space Res., 31, 2055–2060, 2003.

Singer, W., von Zahn, U., and Weiß, J.: Diurnal and annual variations of meteor rates at the arctic circle, Atmos. Chem. Phys., 4, 1355–1363, doi:10.5194/acp-4-1355-2004, 2004.

Sparks, J., Janches, D., Nicolls, M., and Heinselman, C.: Determination of physical and radiant meteor properties using PFISR interferometry measurements of head echoes, J. Atmos. Solar-Terr. Phys., 72, 1221–1230, 2010.

Stober, G.: Astrophysical Studies on Meteors using a SKiYMET All-Sky Meteor Radar, Ph.D. thesis, Institute of Meteorology, University Leipzig, 2009.

Stober, G., Jacobi, C., and Singer, W.: Meteoroid mass determination from underdense trails, J. Atmos. Solar-Terr. Phys., 73, 895–900, 2011.

von Zahn, U.: The total mass flux of meteoroids into the Earth's upper Atmosphere, in: Proceedings of the 17th ESA Symposium on European Rocket and Balloon Programmes and Related Research, Sandefjord, Norway (ESA SP-590), pp. 33–39, 2005.

Westman, A., Wannberg, G., and Pellinen-Wannberg, A.: Meteor head echo altitude distributions and the height cutoff effect studied with the EISCAT HPLA UHF and VHF radars, Ann. Geophys., 22, 1575–1584, doi:10.5194/angeo-22-1575-2004, 2004.

Wyatt, S. and Whipple, F.: The Poynting-Robertson effect on meteor orbits, Astrophysical Journal, 111, 134–141, 1950.